

Astronomical Journal, in press for July 2000

Circumnuclear Supernova Remnants and H II Regions in NGC 253

James S. Ulvestad

*National Radio Astronomy Observatory*¹

P.O. Box O, Socorro, NM 87801

julvesta@nrao.edu

ABSTRACT

Archival VLA data has been used to produce arcsecond-resolution 6- and 20-cm images of the region surrounding the nuclear 200-pc ($\sim 15''$) starburst in NGC 253. Twenty-two discrete sources stronger than 0.4 mJy have been detected within ~ 2 kpc ($\sim 3'$) of the galaxy nucleus; almost all these sources must be associated with the galaxy. None of the radio sources coincides with a detected X-ray binary, so they appear to be due to supernova remnants and H II regions. The region outside the central starburst has a derived radio supernova rate of $\lesssim 0.1$ yr $^{-1}$, and may account for at least 20% of the recent star formation in NGC 253. Most of the newly identified sources have steep, nonthermal radio spectra, but several relatively strong thermal sources also exist, containing the equivalent of tens of O5 stars. These stars are spread over tens of parsecs, and are embedded in regions having average ionized gas densities of ~ 20 – 200 cm $^{-3}$, much lower than in the most active nuclear star-forming regions in NGC 253 or in the super star clusters seen in other galaxies. The strongest region of thermal emission coincides with a highly reddened area seen at near-infrared wavelengths, possibly containing optically obscured H II regions.

Subject headings: galaxies: individual: NGC 253 — galaxies: ISM — galaxies: starburst — radio continuum: galaxies — supernova remnants

1. Introduction

The edge-on spiral galaxy NGC 253 is one of the two prototypical, nearby starburst galaxies (along with M82). Its distance of 2.5 Mpc (Turner & Ho 1985) enables its starburst disk to be

¹The National Radio Astronomy Observatory is a facility of the National Science Foundation, operated under cooperative agreement by Associated Universities, Inc.

studied at very high linear resolution, since $1''$ corresponds to only 12 pc. The galaxy contains an inner starburst disk roughly $15''$ – $20''$ (180–240 pc) in extent that has been studied in detail, especially by virtue of its emission in the infrared (Forbes, Ward, & DePoy 1991; Piña et al. 1992; Keto et al. 1993; Forbes et al. 1993; Kalas & Wynn-Williams 1994; Sams et al. 1994; Böker, Krabbe, & Storey 1998; Keto et al. 1999) and in molecular lines (Canzian, Mundy, & Scoville 1988; Israel, White, & Baas 1995; Jackson et al. 1995; Paglione, Tosaki, & Jackson 1995; Peng et al. 1996; Frayer, Seaquist, & Frail 1998). Subarcsecond-resolution imaging at centimeter wavelengths reveals at least 64 compact radio sources in the inner disk (Turner & Ho 1985; Antonucci & Ulvestad 1988; Ulvestad & Antonucci 1991, 1994, 1997); these are thought to be roughly equally divided between H II regions dominated by thermal emission, and supernova remnants dominated by nonthermal emission (Ulvestad & Antonucci 1997). At the centimeter wavelengths where radio telescopes are most sensitive, the poorer resolution and the increasing strength of the more diffuse galaxy emission lead to confusion that prevents complete source identification in the inner 200-pc starburst.

The 200-pc region clearly dominates the current star formation in NGC 253, as shown by the infrared, millimeter, and centimeter observations. Centimeter imaging of this inner starburst indicates a supernova rate of $\leq 0.3 \text{ yr}^{-1}$ (Ulvestad & Antonucci 1997), which is consistent with results of 0.1 – 0.3 yr^{-1} inferred from models of the infrared emission of the entire galaxy (Rieke et al. 1980; Rieke, Lebofsky, & Walker 1988). Near- and mid-infrared imaging at arcsecond resolution shows a number of emission peaks that do not generally line up with the radio sources (Keto et al. 1993; Sams et al. 1994; Kalas & Wynn-Williams 1994), while Hubble Space Telescope images show at least four compact star clusters, which also do not coincide with individual compact radio sources (Watson et al. 1996). Thus, it is apparent that extinction and confusion play major roles in the inner disk at different wavebands, and it may be that only the centimeter and millimeter images reveal the regions of most recent star formation.

Outside the 200-pc starburst disk, NGC 253 may have a significant amount of star formation, as shown by the existence of larger-scale radio emission (Hummel, Smith, & van der Hulst 1984; Carilli et al. 1992; Beck et al. 1994; Carilli 1996). Since this part of the galaxy is much less affected by confusion and extinction, there is greater potential for identifying the strongest regions of star formation and studying them in multiple bands. However, recent high-resolution studies of the galaxy outside the inner few hundred parsecs are uncommon, since most of the imaging has been of small fields centered on the main starburst disk. One recent study on the larger scale is that of Vogler & Pietsch (1999), who used ROSAT to identify 73 X-ray sources in the bulge, disk, and halo of NGC 253, attributing most of them to X-ray binary stars. To study the population of compact radio sources on this large scale, we have reprocessed the high-resolution 6-cm and 20-cm Very Large Array (VLA) data obtained in 1987 (Antonucci & Ulvestad 1988; Ulvestad & Antonucci 1997) in order to image the entire primary beam of the individual VLA antennas at high resolution; limited computing resources prevented this from being done at the time of the observations. In this paper, we report the locations of the compact radio sources outside the inner 200-pc starburst, compare these locations to images made in other wavebands, and estimate the supernova rate outside the

inner disk.

2. Observations and Data Analysis

The observations of NGC 253 that we use here were made in 1987, using the VLA (Thompson et al. 1980) in its A configuration. Results from imaging the inner starburst at 6 cm (4860 MHz) were reported by Antonucci & Ulvestad (1988), while the 20-cm (1490 MHz) image of the same region was discussed briefly by Ulvestad & Antonucci (1997). Details of the observations were reported in those papers. Other 6-cm observations had much poorer (u,v) coverage than those made in 1987, so only the 1987 data are considered here.

For self-consistency, the data were re-calibrated and self-calibrated using the same procedures reported previously. We then made large-scale (4096×4096 pixels) images of the radio emission of NGC 253 to reveal the compact radio sources seen throughout the primary beam of the individual 25-m telescopes of the VLA. These images covered $26' \times 26'$ at 20 cm and $8' \times 8'$ at 6 cm. Outside the starburst disk, confusion was not a significant issue, but sensitivity was critical. We therefore used natural weighting of the data in the (u,v) plane (Sramek & Schwab 1989; Briggs, Schwab, & Sramek 1999); this scheme produces the maximum sensitivity, at the price of a modest loss in resolution. A zero-spacing (total) flux density was specified in the imaging, in order to partially compensate for the lack of short interferometer spacings. This reduced, but did not completely remove, systematic effects caused by diffuse emission that was not sampled well in our observations.

Table 1 gives the resolution and the r.m.s. noise achieved for the final images. Several effects contribute to reductions in the sensitivity far from the field center; each is discussed briefly here. First, the attenuation of the primary beam of the individual VLA antennas reduces the sensitivity by more than 10% at 6 cm and 20 cm for respective distances from the pointing direction of greater than $1.7'$ and $5.4'$. Corrections for this attenuation were made using the AIPS (van Moorsel, Kemball, & Greisen 1996) software developed by NRAO, and were less than 10% except for several sources (see Section 4.1) far from the main area of radio emission. A second effect, chromatic aberration (“bandwidth smearing”) due to the non-zero observing bandwidth (Bridle & Schwab 1999), is more deleterious. It reduces the peak flux density by more than a factor of two at distances greater than $2'$ from the phase center, and is progressively worse farther out in the field. The actual phase center of the observations was $\sim 10''$ north of the apparent galaxy nucleus, at a B1950 position of $(\alpha, \delta) = (00^h 45^m 05.^s 80, -25^\circ 33' 29.^'' 0)$; since most of the large-scale sources are north of the nucleus, this actually was slightly beneficial in the final data analysis. Compared to the chromatic aberration, the reduction in flux density due to delay smearing (Bridle & Schwab 1999) over the observations’ 10-second averaging period is negligible. Finally, the lack of short interferometer spacings causes correlated positive or negative emission as high as 0.08–0.1 mJy over areas of $\sim 50 \times 50$ pixels away from the center of the field. The final source detection threshold that was used was four times the quadrature sum of this systematic value and the r.m.s. noise, or approximately 0.4 mJy at each wavelength. However, this threshold rises substantially at distances

more than a few arcminutes from the phase center.

3. Images and Source Identification

Figure 1 is a portion of the 20-cm image showing the circumnuclear region of NGC 253 at high resolution. The locations of compact X-ray sources detected by Vogler & Pietsch (1999), using the ROSAT High Resolution Imager, are shown as crosses whose sizes indicate the errors in the X-ray positions. We have identified all radio sources that have apparent peak flux densities of at least $0.4 \text{ mJy beam}^{-1}$ at either 6 cm or 20 cm, outside the central 200-pc starburst. Figures 2a and 2b are respective enlargements of the 20-cm and 6-cm images showing the radio emission from the 200-pc starburst disk and its surroundings, including a number of the circumnuclear compact sources. Note that the 6-cm image shows little detail, due to the larger number of beam areas needed to cover the given region, but it does serve to illustrate the relative locations of the detected sources.

Table 2 lists the source identifications in the circumnuclear region at the two wavelengths. (Each source listed in this table can be seen in the region shown in Figure 1.) Included are the source positions, flux densities at 6 cm and 20 cm, measured sizes, and a few comments. When compact sources are identified at both wavelengths, the higher resolution 6-cm position is quoted; typical position accuracies are $0.^{\prime\prime}1$ – $0.^{\prime\prime}2$. At 6 cm, flux densities as low as 0.2 mJy are given for sources that meet the 0.4-mJy threshold at 20 cm, but these flux densities have very large fractional errors. Source flux densities and sizes have been derived by making Gaussian fits to the individual sources in the image plane, and confirmed by integrating over the region of significant emission. Most sources are unresolved in the full-resolution images at both 6 cm and 20 cm, as indicated by a “U” in the table. The sizes of resolved sources are derived from the 6-cm full-resolution image. The total 6-cm flux densities and approximate sizes found at full resolution generally are consistent with values found from a 6-cm image tapered to the 20-cm resolution.

We estimated flux density errors due to several causes. First, the areas of apparent systematic negative or positive flux near the main starburst disk, caused by undersampling in the aperture plane, average as much as $0.08 \text{ mJy beam}^{-1}$ at 6 cm and $0.10 \text{ mJy beam}^{-1}$ at 20 cm; this offset is denoted by σ_o . Second, there is a $\sim 5\%$ error in the absolute flux density scales of each of the two maps, so $\sigma_{sc} = 0.05S$, where S is the source flux density. Third, there is a fitting error, σ_f , caused by confusion with underlying diffuse emission and uncertainties in the source fits. Since the newly identified sources reported here are outside the main starburst disk and fairly well isolated, we take the confusion error to be negligible, so σ_f is simply the uncertainty reported by the least-squares fitting program. This value includes the r.m.s. noise given in Table 1, so the noise is not included separately. We combine these errors in quadrature to get the total flux-density error, σ , using

$$\sigma^2 = \sigma_o^2 + (0.05S)^2 + \sigma_f^2. \quad (1)$$

Thus, the total flux-density error for a 0.4-mJy source is typically 0.09 mJy at 6 cm and 0.11 mJy

at 20 cm.

4. Discussion

4.1. Are All Detected Sources Associated with NGC 253?

There are 22 sources above the 0.4-mJy limit at 20 cm, inside a box $4'$ (2.8 kpc) on a side and centered on the nucleus of NGC 253. The density of background sources above this flux-density threshold is expected to be $\sim 10^6 \text{ sr}^{-1}$ (Windhorst et al. 1985). Therefore, we expect about one background source stronger than 0.4 mJy within a field of 16 square arcminutes, implying that almost all of the detected sources are associated with NGC 253. The apparent lack of weak sources at greater distances from the nucleus may be caused primarily by chromatic aberration (see Section 2); sources far from the phase center of the observation have their peak flux densities reduced substantially, and therefore may fall below the detection threshold. Observations using narrow spectral-line channels rather than a broadband continuum would be needed to determine whether other weak compact sources exist farther from the phase center.

Five additional sources were detected at 20 cm within an area $12'$ on a side, centered on NGC 253, and are listed in Table 3. These are within the size of the optical galaxy, which has a measured diameter of $25'$ to 25th magnitude (de Vaucouleurs et al. 1991). Images of these sources are not shown, since they are substantially degraded by chromatic aberration, which prevents measurement of the source sizes. Therefore, only the total flux densities are given in Table 3. The source locations are best seen in previous lower-resolution radio images of NGC 253, particularly that published by Anantharamaiah & Goss (1990), though none of those images resolves source B2 into the three components distinguished here. Only sources much stronger than 0.4 mJy can be detected in the large region due to the chromatic aberration. The expected density of sources stronger than 15 mJy at 20 cm is $\sim 10^4 \text{ sr}^{-1}$ (Windhorst et al. 1985), so we expect to detect less than one background source above this threshold. Source B3 appears to be associated with a “spur” noted by Carilli et al. (1992), and the three-component source B2 lies along the large-scale galaxy disk, making it probable that at least B2 and B3 are associated with NGC 253.

4.2. Circumnuclear Star Formation

The detected circumnuclear sources (Table 2) outside the central starburst have typical flux densities of 0.4–3 mJy at 6 cm and 20 cm, corresponding to radio powers of 3×10^{17} to $2 \times 10^{18} \text{ W Hz}^{-1}$. Most of them seem to have relatively steep spectra; for a source with a flux density of 0.4 mJy at 6 cm and a spectral index of -0.7 (with $S_\nu \propto \nu^{+\alpha}$), the total luminosity between 10 MHz (or 100 MHz) and 100 GHz is $\sim 1.1 \times 10^{35} \text{ erg s}^{-1}$. This luminosity is a factor of 100–1000 lower than the luminosities of the point X-ray sources detected by Vogler & Pietsch (1999), which

they generally attribute to X-ray binaries. Since none of the radio sources listed in Table 2 coincides with a compact X-ray source, the radio emission is probably not associated with evolved binaries.

In the main 200-pc starburst disk of NGC 253, Antonucci & Ulvestad (1988) deduced that ~ 100 compact radio sources exist. A supernova rate of $\leq 0.3 \text{ yr}^{-1}$ was estimated from the radio emission (Ulvestad & Antonucci 1997), while supernova rates of $0.1\text{--}0.3 \text{ yr}^{-1}$ have been derived on other grounds (Rieke et al. 1980; Rieke, Lebofsky, & Walker 1988). Here, we report an additional 22 circumnuclear compact radio sources that lie outside the central 200-pc starburst, but within 2 kpc ($170''$) of the galaxy center. Since they do not coincide with X-ray binaries, and most are less than 5–10 pc ($0.''4\text{--}0.''8$) in diameter, they most likely are due to supernova remnants and H II regions, as are the sources in the nuclear region. The sources can be compared to the galactic supernova remnant Cas A. For an assumed distance of 2.8 kpc (van den Bergh 1971) and a flux density of $\sim 500 \text{ Jy}$ (Baars et al. 1977), Cas A has a 6-cm radio power of $\sim 5 \times 10^{17} \text{ W Hz}^{-1}$, comparable to the powers of the weaker circumnuclear sources in NGC 253.

There are 10–15 circumnuclear sources with steep radio spectra, likely to be supernova remnants. The number of steep-spectrum sources is uncertain because some are too weak for good spectral-index determination. In addition, since the (u, v) coverage at 6 cm is not matched to that at 20 cm, more flux density may be “resolved out” at 6 cm, which could lead to estimates of spectra that are overly steep. (This resolution effect is the primary reason that spectral indices are not quoted in Table 2.) By comparison, there are at least 32 steep-spectrum sources in the inner 200-pc starburst (Ulvestad & Antonucci 1997); correcting for confusion would probably increase this number to 50 or more. If the circumnuclear radio sources have the same general character as those in the main starburst disk, a simple comparison with the analysis of Ulvestad & Antonucci (1997) indicates that the estimated circumnuclear supernova rate outside the central starburst is $\lesssim 0.1 \text{ yr}^{-1}$. (Of course, some sources outside the strong starburst could have been missed, due primarily to chromatic aberration.) In any case, based solely on the ratio of steep-spectrum sources inside and outside the 200-pc starburst, we infer that at least 20%–30% of the global star-formation and supernova remnants are outside that central starburst. No supernovae have been detected in the circumnuclear region during limited searches made at optical wavelengths in 1988–1991 (Richmond, Filippenko, & Galisky 1998), and at near-infrared wavelengths in late 1993 (Grossan et al. 1999). However, such searches did not cover long enough time periods to expect supernova detections in NGC 253, and also could have been affected by obscuration and confusion.

Figure 3 shows a complex of sources to the west of the main starburst disk, roughly 800 pc from the galaxy nucleus. Figure 3a is the 20-cm image, showing four individual radio sources. These sources are numbered 4, 6, 7, and 8 in Table 2 and similarly labeled in the figure. Two 6-cm images also are shown. Figure 3b is an image for which the visibility data were tapered and then restored with a point-spread function identical to that at 20 cm, while Figure 3c is a full-resolution image. Inspection of Table 2 reveals that the two strongest 6-cm sources shown in Figure 3b have flat or inverted spectra. Summing the four individual compact sources gives a total 6-cm flux density of $6.6 \pm 0.4 \text{ mJy}$ and a total 20-cm flux density of $8.3 \pm 0.4 \text{ mJy}$, while integration of the images over

the region of Figure 3 yields a total 6-cm flux density of 7.7 mJy and a total 20-cm flux density of 9.0 mJy, slightly higher than the fits to the compact sources.

We take the somewhat simplistic step of making a two-component decomposition of the flux density in the radio sources shown in Figure 3. To do so, we assume the presence of a thermal, flat-spectrum component having $\alpha = -0.1$, and a nonthermal, steep-spectrum component due to supernova remnants. The steep-spectrum sources in the inner starburst of NGC 253 have typical spectral indices of $\alpha = -0.7$ (Ulvestad & Antonucci 1997), while galactic supernova remnants have a median spectral index of $\alpha = -0.5$ (Green 1996), so there is some range in the estimates of the flat-spectrum component. The simple spectral decomposition gives thermal radio emission containing 5.3 to 5.9 mJy out of a total of 6.6 mJy at 6 cm, for a steep-spectrum component having a spectral index ranging from -0.5 to -0.7 . Thus, 80% to 90% of the 6-cm flux density in the region shown in Figure 3 appears to be thermal in origin.

The natural conclusion is that the flat-spectrum radio component is thermal radiation from H II regions energized by young stars. Applying the analysis of the strongest flat-spectrum source in the starburst disk, which was described by Ulvestad & Antonucci (1997), we find that the equivalent of ~ 70 O5 stars is necessary to energize the radio emission within a region of about $12'' \times 10''$ (144 \times 120 pc). This is comparable to the number of young stars needed to account for the strongest thermal source in the inner starburst, but those stars are contained in a volume $\sim 6 \times 10^5$ times higher. Therefore, the average thermal gas density in the 130-pc region shown in Figure 3 is ~ 20 cm $^{-3}$, much lower than the values of $\sim 10^4$ cm $^{-3}$ found in the dense part of the inner starburst of NGC 253 (Ulvestad & Antonucci 1997) and in NGC 5253 (Turner, Ho, & Beck 1998), or of $\sim 10^3$ cm $^{-3}$ for the typical thermal radio sources in NGC 4038/4039 (Neff & Ulvestad 2000).

Few high-resolution observations at other wavelengths are available for the region shown in Figure 3. However, a moderate-resolution ($9'' \times 17''$) VLA image (Carilli 1996) shows a source at the same location, with an apparent 3.6-cm flux density between 5 and 6 mJy. This is entirely consistent with the value expected for the flat-spectrum component deduced above. Near-infrared images shown in Figures 1 and 10 of Engelbracht et al. (1998) indicate a slight enhancement in K (2.2 μ m) at the location of the complex of compact radio sources, apparently along an inner spiral arm. This infrared source may represent a highly reddened set of H II regions containing the numerous young stars that energize the local radio complex.

A similar argument can be made for source 15, which lies nearly 2 kpc from the galaxy nucleus, and also appears to have a thermal spectrum. Ionization of this radio source requires the equivalent of about 35 O5 stars in a region about 15–30 pc in diameter, and an average ionized density near 200 cm $^{-3}$. Chromatic aberration makes these estimates somewhat uncertain, but they should be correct to 50% or better.

The relatively low average densities derived for the two strongest thermal-emitting complexes in the circumnuclear region imply that they contain more “normal” star formation, rather than the

intense starbursts characteristic of the central 200 parsecs. The number and the density of massive young stars are significantly higher than in Orion and other nearby Galactic O-B associations (Blaauw 1964), and may be comparable to the richest star-forming regions in our Galaxy, such as W49 (Welch 1993; de Pree, Mehringer, & Goss 1997). However, the intensity of massive star formation is considerably lower than in 30 Doradus (Hunter et al. 1995) or in the super star clusters seen in a number of starburst galaxies (O’Connell, Gallagher, & Hunter 1994; Schweizer & Seitzer 1998; Turner, Ho, & Beck 1998; Whitmore et al. 1999; Kobulnicky & Johnson 1999; Neff & Ulvestad 2000).

5. Summary

We have used archival VLA data to image the circumnuclear region of NGC 253 at arcsecond resolution. Twenty-two compact radio sources have been found in the inner 2 kpc of the galaxy, but outside the well-known 200-pc disk, and most of these are probably associated with regions of recent star formation. The supernova rate inferred outside the central starburst is $\lesssim 0.1 \text{ yr}^{-1}$; this may be a slight underestimate due to the decreasing sensitivity of the radio observations at distances more than $\sim 2'$ from the nucleus. Therefore, the region outside the well-studied inner starburst seems to account for a significant fraction of the recent star formation in NGC 253. A collection of sources located 800 pc to the west of the nucleus appears to be a complex of H II regions energized by the equivalent of 70 O5 stars, but with an average ionized gas density $\sim 10^3$ times lower than that found in the inner starburst of the galaxy.

I thank K. Anantharamaiah, R. Antonucci, N. Mohan, and W. Pietsch for useful discussions and for providing data in advance of publication. I especially thank the referee, Jean Turner, for some perceptive comments and for pointing out errors in Table 2. This research has made use of the NASA/IPAC Extragalactic Database (NED) which is operated by the Jet Propulsion Laboratory, California Institute of Technology, under contract with the National Aeronautics and Space Administration. In addition, this research has made use of NASA’s Astrophysics Data System.

REFERENCES

Anantharamaiah, K. R., & Goss, W. M. 1990, in IAU Colloq. 125, Radio Recombination Lines: 25 Years of Investigations, ed. M. A. Gordon & R. L. Sorochenko (Dordrecht: Kluwer), 267

Antonucci, R. R. J., & Ulvestad, J. S. 1988, *ApJ*, 330, L97

Baars, J. W. M., Genzel, R., Pauliny-Toth, I. I. K., & Witzel, A. 1977, *A&A*, 61, 99

Beck, R., Carilli, C. L., Holdaway, M. A., & Klein, U. 1994, *A&A*, 292, 409

Blaauw, A. 1964, *ARA&A*, 2, 213

Böker, T., Krabbe, A., & Storey, J. W. V. 1998, *ApJ*, 498, L115

Bridle, A. H., & Schwab, F. R. 1999, in Synthesis Imaging in Radio Astronomy II, ASP Conf. Series 180, ed. G. B. Taylor, C. L. Carilli, & R. A. Perley (San Francisco: ASP), 371

Briggs, D. S. Schwab, F. R., & Sramek, R. A. 1999, in Synthesis Imaging in Radio Astronomy II, ASP Conf. Series 180, ed. G. B. Taylor, C. L. Carilli, & R. A. Perley (San Francisco: ASP), 127

Canzian, B., Mundy, L. G., & Scoville, N. Z. 1988, *ApJ*, 333, 157

Carilli, C. L. 1996, *A&A*, 305, 402

Carilli, C. L., Holdaway, M. A., Ho, P. T. P., & de Pree, C. G. 1992, *ApJ*, 399, L59

de Pree, C. G., Mehringer, D. M., & Goss, W. M. 1997, *ApJ*, 482, 307

de Vaucouleurs, G., de Vaucouleurs, A., Corwin, H. G., Jr., Buta, R. J., Paturel, G., & Fouqué, P. 1991, Third Reference Catalogue of Bright Galaxies (New York: Springer)

Engelbracht, C. W., Rieke, M. J., Rieke, G. H., Kelly, D. M., & Achtermann, J. M. 1998, *ApJ*, 505, 639

Forbes, D. A., Ward, M. J., & DePoy, D. L. 1991, *ApJ*, 380, L63

Forbes, D. A., Ward, M. J., Rotaciuc, V., Blietz, M., Genzel, R., Drapatz, S., van der Werf, P. P., & Krabbe, A. 1993, *ApJ*, 406, L11

Frayer, D. T., Seaquist, E. R., & Frail, D. A. 1998, *AJ*, 115, 559

Green, D. A. 1996, in IAU Colloq. 145, Supernovae and Supernova Remnants, ed. R. McCray & Z. Wang (Cambridge: Cambridge University Press), 419

Grossan, B., Spillar, E., Tripp, R., Pirzkal, N., Sutin, B. M., Johnson, P., & Barnaby, D. 1999, *AJ*, 118, 705

Hummel, E., Smith, P., & van der Hulst, J. M. 1984, *A&A*, 137, 138

Hunter, D. A., Shaya, E. J., Holtzman, J. A., Light, R. M., O’Neil, E. J., & Lynds, R. 1995, *ApJ*, 448, 179

Israel, F. P., White, G. J., & Baas, F. 1995, *A&A*, 302, 343

Jackson, J. M., Paglione, T. A. D., Carlstrom, J. E., & Rieu, N.-Q. 1995, *ApJ*, 438, 695

Kalas, P., & Wynn-Williams, C. G. 1994, *ApJ*, 434, 546

Keto, E., Ball, R., Arens, J., Jernigan, G., Meixner, M., Skinner, C., & Graham, J. 1993, *ApJ*, 413, L23

Keto, E., Hora, J. L., Fazio, G. G., Hoffmann, W., & Deutsch, L. 1999, *ApJ*, 518, 183

Kobulnicky, H. A., & Johnson, K. E. 1999, *ApJ*, 527, 154

Neff, S. G., & Ulvestad, J. S. 2000, *AJ*, submitted

O’Connell, R. W., Gallagher, J. S., & Hunter, D. A. 1994, *ApJ*, 433, 65

Paglione, T. A. D., Tosaki, T., & Jackson, J. M. 1995, *ApJ*, 454, L117

Peng, R., Zhou, S., Whiteoak, J. B., Lo, K. Y., & Sutton, E. C. 1996, *ApJ*, 470, 821

Piña, R. K., Jones, B., Puetter, R. C., & Stein, W. A. 1992, *ApJ*, 401, L75

Richmond, M. W., Filippenko, A. V., & Galinsky, J. 1998, *PASP*, 110, 553

Rieke, G. H., Lebofsky, M. J., Thompson, R. I., Low, F. J., & Tokunaga, A. T. 1980, *ApJ*, 238, 24

Rieke, G. H., Lebofsky, M. J., & Walker, C. E. 1988, *ApJ*, 325, 679

Sams, B. J., Genzel, R., Eckart, A., Tacconi-Garman, L., & Hofmann, R. 1994, *ApJ*, 430, L33

Schweizer, F., & Seitzer, P. 1998, *AJ*, 116, 2206

Sramek, R. A., & Schwab, F. R. 1989, in *Synthesis Imaging in Radio Astronomy*, ASP Conf. Series 6, ed. R. A. Perley, F. R. Schwab, & A. H. Bridle (San Francisco: ASP), 117

Thompson, A. R., Clark, B. G., Wade, C. M., & Napier, P. J. 1980, *ApJS*, 44, 151

Turner, J. L., & Ho, P. T. P. 1985, *ApJ*, 299, L77

Turner, J. L., Ho, P. T. P., & Beck, S. C. 1998, *AJ*, 116, 1212

Ulvestad, J. S., & Antonucci, R. R. J. 1991, *AJ*, 102, 875

Ulvestad, J. S., & Antonucci, R. R. J. 1994, *ApJ*, 424, L29

Ulvestad, J. S., & Antonucci, R. R. J. 1997, *ApJ*, 488, 621

van den Bergh, S. 1971, *ApJ*, 165, 259

van Moorsel, G., Kemball, A., & Greisen, E. 1996, in *Astronomical Data Analysis Software and Systems V*, ASP Conf. Series 101, ed. G. H. Jacoby & J. Barnes (San Francisco: ASP), 37

Vogler, A., & Pietsch, W. 1999, *A&A*, 342, 101

Watson, A. M., et al. 1996, *AJ*, 112, 534

Welch, W. J. 1993, in *Massive Stars: Their Lives in the Interstellar Medium*, ASP Conf. Series 35, ed. J. P. Cassinelli & E. B. Churchwell (San Francisco: ASP), 15

Whitmore, B. C., Zhang, Q., Leitherer, C., Fall, S. M., Schweizer, F., & Miller, B. W. 1999, *AJ*, 118, 1551

Windhorst, R. A., Miley, G. K., Owen, F. N., Kron, R. G., & Koo, D. C. 1985, *ApJ*, 289, 494

Table 1. Full-Resolution Image Parameters

λ (cm)	Date	Beam Size			r.m.s. noise ($\mu\text{Jy beam}^{-1}$)
		Major ($''$)	Minor ($''$)	P.A. ($^{\circ}$)	
6	87JUL10	0.86	0.51	2	27
20	87JUL21	2.77	1.72	7	41

Table 2. Compact Circumnuclear Sources

No.	Position		Flux Density (mJy)		Source Size ^a (arcsec)
	α (1950)	δ (1950)	6 cm	20 cm	
1	00 ^h 44 ^m 59. ^s 404	−25°33'59.07	0.4 ± 0.1	0.6 ± 0.1	U
2	00 44 59.498	−25 33 54.91	0.3 ± 0.1	0.7 ± 0.1	U
3	00 45 00.117	−25 34 20.89	0.2 ± 0.1	0.6 ± 0.1	U
4 ^b	00 45 00.580	−25 33 37.30	0.7 ± 0.2	2.3 ± 0.2	0.9 × 0.7, 89°
5	00 45 00.619	−25 34 15.25	< 0.2	0.4 ± 0.1	U
6	00 45 00.785	−25 33 35.66	2.4 ± 0.2	2.8 ± 0.2	1.1 × 0.9, 7°
7	00 45 01.007	−25 33 31.19	1.2 ± 0.1	1.8 ± 0.2	0.6 × 0.6
8	00 45 01.187	−25 33 35.61	2.3 ± 0.2	1.4 ± 0.1	1.9 × 1.5, 145°
9	00 45 02.495	−25 34 00.40	1.2 ± 0.1	3.5 ± 0.2	U
10	00 45 02.659	−25 33 04.87	< 0.2	0.4 ± 0.1	U
11	00 45 03.346	−25 32 59.96	0.4 ± 0.1	0.9 ± 0.1	U
12	00 45 03.497	−25 33 00.15	< 0.2	0.6 ± 0.1	U
13	00 45 04.236	−25 32 46.97	0.3 ± 0.1	0.5 ± 0.1	U
14	00 45 05.998	−25 32 29.16	0.2 ± 0.1	0.4 ± 0.1	U
15 ^c	00 45 06.097	−25 31 55.60	2.7 ± 0.3	2.4 ± 0.3	...
16	00 45 06.153	−25 32 26.66	0.5 ± 0.1	0.6 ± 0.1	U
17	00 45 09.602	−25 33 55.91	< 0.2	0.5 ± 0.1	U
18 ^b	00 45 09.804	−25 33 06.73	1.5 ± 0.1	3.9 ± 0.2	1.2 × 0.9, 2°
19 ^c	00 45 12.084	−25 32 56.00	0.4 ± 0.2	2.4 ± 0.3	...
20 ^c	00 45 13.136	−25 33 00.97	2.7 ± 0.2	6.1 ± 0.3	...
21	00 45 13.308	−25 33 08.83	< 0.2	0.6 ± 0.1	U
22 ^c	00 45 15.846	−25 32 01.53	0.9 ± 0.2	1.2 ± 0.2	...

^aSource sizes denoted as “U” are unresolved.

^bSource is significantly larger at 20 cm than at 6 cm. Derived spectral index may be too steep, because of resolution effects at 6 cm.

^cSource has significant primary beam correction and chromatic aberration, causing uncertainties in the source flux densities and structure. Only the total flux densities have been measured, and the 6-cm flux density may be an underestimate.

Table 3. Wide-Field Radio Sources^a

No.	Position		Flux Density (mJy)		Comments
	α (1950)	δ (1950)	6 cm	20 cm	
B1	00 ^h 44 ^m 45. ^s 07	−25°34'05.5"	...	16 ± 3	Outside 6 cm window
B2a	00 45 17.08	−25 29 58.6	< 2	5 ± 1	Undetected at 6 cm
B2b	00 45 17.45	−25 29 59.7	1.7 ± 0.3	...	Blends with B2c at 20 cm
B2c	00 45 17.54	−25 30 00.6	5.2 ± 0.8	18 ± 3	Blends with B2b at 20 cm
B3	00 45 31.33	−25 34 52.6	...	50 ± 8	Outside 6 cm window

^aSource sizes are unknown, due to severe chromatic aberration.

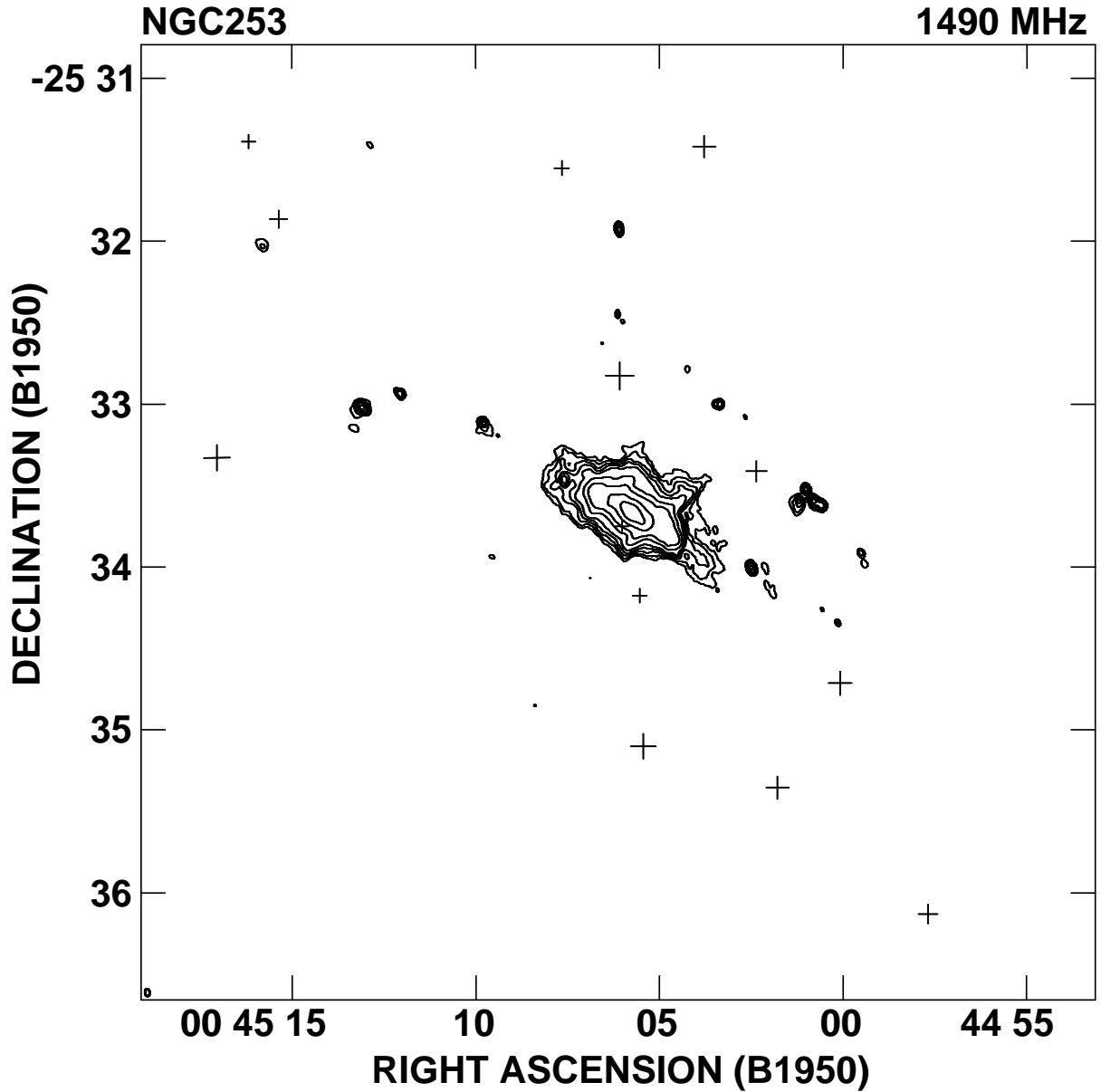


Fig. 1.— Wide-field image of NGC 253 at 20 cm. Contour levels are at $-1, 1, 1.4, 2, 2.8, 4, 8, 16, 64$, and 256 times $300 \mu\text{Jy beam}^{-1}$; no negative contours are present in the image. The peak flux density is $271 \text{ mJy beam}^{-1}$, and the restoring beam of $2.^{\circ}77 \times 1.^{\circ}72$ in position angle 7° is indicated by the minuscule ellipse in the lower-left corner. X-ray sources detected by the ROSAT HRI (Vogler & Pietsch 1999) are indicated as crosses, with the sizes of the crosses showing their positional uncertainty.

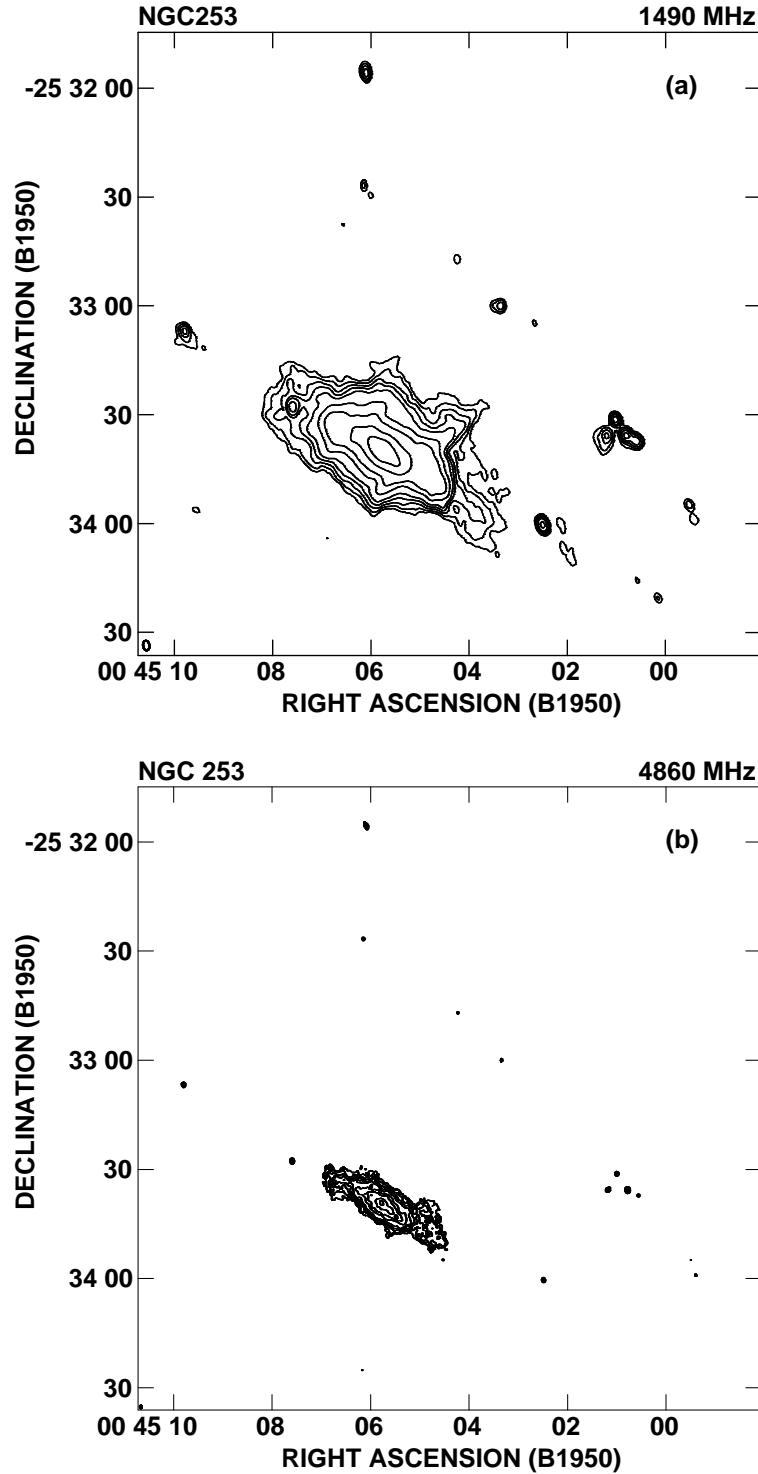


Fig. 2.— Enlargements of 20-cm and 6-cm full-resolution images near the main starburst disk of NGC 253. (a) 20-cm image, with restoring beam and contour levels as in Figure 1. (b) 6-cm image, with contour levels at $-1, 1, 1.4, 2, 2.8, 4, 8, 16, 64$, and 256 times $200 \mu\text{Jy beam}^{-1}$. The peak flux density is 97 mJy beam^{-1} , and the restoring beam (lower left) is $0.^{\prime\prime}86 \times 0.^{\prime\prime}51$ in position angle 2° .

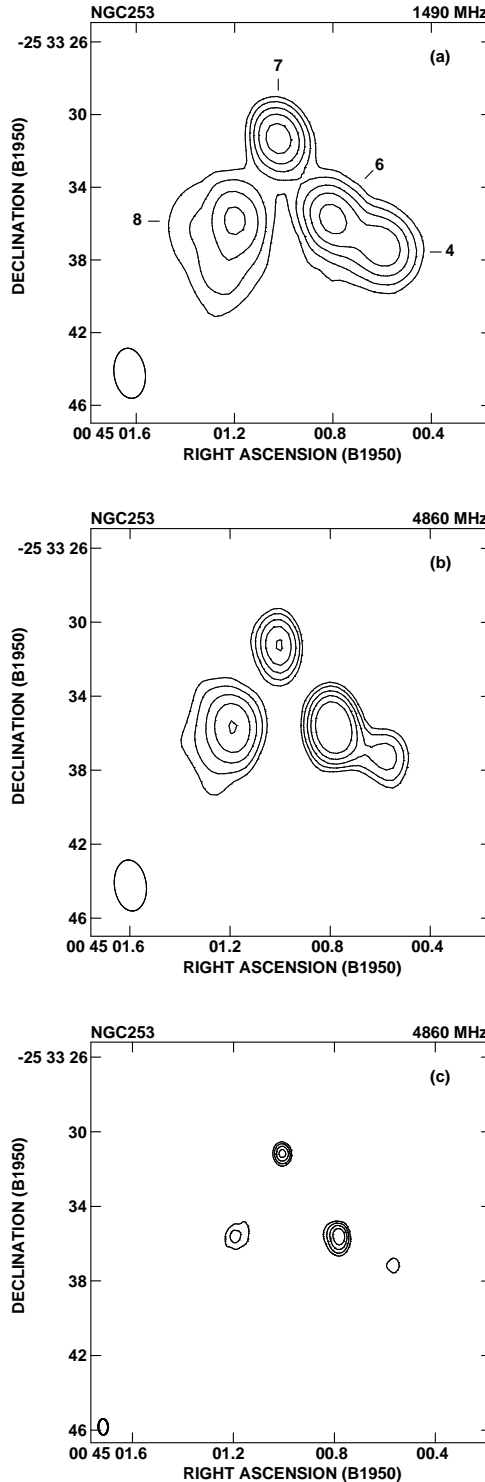


Fig. 3.— Enlargements of a complex of sources to the west of the main starburst disk. (a) 20-cm image, with contour levels of $-1, 1, 1.4, 2, 2.8$, and 4 times $300 \mu\text{Jy beam}^{-1}$. (b) 6-cm image, tapered to the same resolution as the 20-cm image, with contour levels of $-1, 1, 1.4, 2, 2.8$, and 4 times $200 \mu\text{Jy beam}^{-1}$. (c) 6-cm full resolution image, with the same contour levels and restoring beam as in Figure 3b.